Eco-friendly synthesis of self-supported N-doped Sb_2S_3-carbon fibers with high atom utilization and zero discharge for commercial full lithium-ion batteries

Hong Yin,[†, §, ‡] Kwan San Hui,[⊥] Xun Zhao,[‡] Shiliang Mei,[§] Xiaowei Lv,[*, †] Kwun Nam Hui,[*, §] Jun Chen[*, ‡]

[†]College of Materials and Chemical Engineering, Key Laboratory of Inorganic Nonmetallic Crystalline and Energy Conversion Materials, China Three Gorges University, Yichang 443002, China

[§]Institute of Applied Physics and Materials Engineering, University of Macau, Avenidada Universidade, Taipa, Macau, China

[‡]Department of Bioengineering, University of California, Los Angeles, Los Angeles, CA 90095, USA

[⊥]School of Mathematics, University of East Anglia, Norwich NR4 7TJ, UK

*Corresponding Authors

E-mail: xwlv@ctgu.edu.cn (X. L.);

bizhui@um.edu.mo (K.N.H.);

jun.chen@ucla.edu (J. C.).

ABSTRACT

Antimony trisulfide (Sb_2S_3) is a prospective electrode material for lithium-ion batteries (LIBs) because of its thermal stability, low price and high specific capacity. However, the commercialization of the Sb_2S_3 as an anode material is greatly hindered by its poor electronic conductivity and massive volume variation during charge/discharge cycles. Moreover, growing demand in reducing greenhouse gas emissions requires the materials preparation process to be pollution-free and high energy-efficient. Herein, we introduce, for the first time, an eco-friendly and highly efficient one-step annealing method to construct a 3D flexible conductive network and buffer matrix for N-doped Sb_2S_3-carbon fibers (NSSCs) as a high-performance anode. It is assembled by mixing sulfur and antimony in atomicity level with stoichiometric ratio as the electrospinning precursor and then annealed in sealed quartz tube to assure the high atom utilization of nitrogen and sulfur. Benefiting from the 3D structure and compositional advantages, the NSSCs electrode with improved conductivity and carbon buffer matrix exhibits superior Li-storage performance. As a result, this work not only promotes the commercialization of antimony trisulfide but also points out a general eco-friendly method, which can be widely applied to synthesize a variety of flexible metal sulfides and metal nitrides with high atom utilization and zero discharge.

KEYWORDS: high atom utilization, zero discharge, volume expansion, eco-friendly, energy storage.

INTRODUCTION.

Traditional energy storage devices, such as alkaline batteries, nickel-metal hydride batteries and fuel cell have been gradually substituted by the lithium-ion batteries (LIBs) because of their long-term cycling life and high energy density.[1-3] Together with additional features, such as being environmentally friendly, no memory effect and wide temperature applicability, LIBs are extensively used for intelligent devices, power sources and uninterrupted power supply system.[4, 5] Moreover, the ever-increasing energy storage markets puts forward demanding applications on high power and high energy density LIBs.[6-8] High-performing anode materials with excellent specific capacity and long cycle lifetime are always restricted and highly desired in the LIBs community. Graphite, generally, is a commonly-used anode material for energy storage, but its distinct advancement was largely shadowed by its minor theoretical specific capacity of 370 mA h g^{-1}, limited power density due to the serious capacity loss under high-rate cycles.[9]

Antimony trisulfide (Sb_2S_3) with high capacity, thermal stability and low price, recently has been developing a hopeful material for solar cells,[10] light irradiation,[11] chalcogenide glasses,[12] and electrochemical energy storage.[13, 14] However, the charge-discharge process of Sb_2S_3 is generally coupled with volume expansive deformation. And it will accompany with continuous formation and collapsing of solid electrolyte interface (SEI), giving rise to a rapid capacity weakening in the cycle performance.[15-18] Combining highly conductive carbon with active nanomaterials may be an effective strategy to address the volume expansion and low electrical conductivity of Sb_2S_3.[19, 20]

And bundle-like Sb_2S_3 materials,[21] imbedded ultrafine Sb_2S_3 nanoparticles in mesoporous carbon spheres,[22] Sb_2S_3/C/Si composite fibers,[23] have been reported to advance the practicability of the Sb_2S_3 for LIBs. However, the finite boost for capacity and cycling life of these materials hardly cannot accommodate the budget needs. Furthermore, in the Sb_2S_3 based battery community, few reports are focused on the full cell performance, leading to a disjointedness in practical application. Thus, lots of enhancements in nano material preparation and long cycling life of the promising Sb_2S_3 material are deeply urgent. Furthermore, the poor intrinsic conductivity of Sb_2S_3 also severely impedes its electrontransport and rate performance.[24-26] And the preparation process of Sb_2S_3 based active materials usually accompanies with S, Se and heavy metals discharge, which results in a waste of raw materials and serious environment pollution.[27] Therefore, an ideal green synthesis method with low pollution and 100% utilization of reactant atoms is very imperative to commercialize the Sb_2S_3 materials for LIBs. In addition, the rapid advancement of wearable devices requires flexible and sustainable energy supply, which is also beyond the capability of conventional rigid batteries.[28-35]

Herein, in this work, we developed N-doped Sb_2S_3 fibers (NSSCs) as an eco-friendly and resource-conserving strategy to successfully address the common issues of poor conductivity, large volume expansion in Sb_2S_3 anode materials for LIBs. And a flexible full battery was also developed via coupling with the cathode material of α-$NaFeO_2$ Al_2O_3-$LiNi_{0.8}Co_{0.15}Al_{0.05}O_2$. The NSSCs were assembled by mixing sulfur and antimony in atomicity level with stoichiometric ratio as the electrospinning precursor.

Annealing in sealed quartz tube assures the high atom utilization and zero discharge for nitrogen and sulfur. The 1D nanofiber form can alleviate the volume expansion process and facilitate the electrolyte infiltrating the interior region of anode material, contributing to superior Li-storage performance for LIBs. Furthermore, for binder-free anode, the creation of arrayed 1D nanofiber framework could deliver high-speed channels for electronic transportation, which can access the properties of metal current collector. The NSSCs electrode also shows improved conductivity and superior electrochemistry performance due to the carbon buffer matrix. The NSSCs electrode is demonstrated to contribute a capacity of 490.3 mA h g^{-1} after 1000 cycles and a rate capacity of 336 mA h g^{-1} at a current density of 8 A g^{-1} and even sustained a capacity of 600 mA h g^{-1} at a current rate of 0.5 C after 200 cycles for the flexible full battery. This work represents a great advancement in the development and commercialization for high-preforming antimony trisulfide anode materials.

RESULTS AND DISCUSSION

The preparation details of Sb_2S_3 carbon fibers (NSSCs) composite are shown in **Figure 1**a-c. Typically, the PVA and PAN fibers are carbonized and the Sb source is decomposed at a high temperature.[36] The antimony ions and valid heat-treatment accelerate the transformation of precursor and the carbon nanofiber matrix further limits the development of antimony nanoparticles. As a result, the Sb grains are uniformly embedded in the carbon nanofibers. It's worth noting that the pyrolytic by-products may be ammonia, water and carbon dioxide.[37, 38] The ammonia can be induced to the production of nitrogen and hydrogen free radicals. Following this process, the nitrogen

free radical can be coerced into the carbon fibers forming an N-doping system in a sealed quartz tube under high temperature and high pressure (**Figure 1**b). Meanwhile, sulfur atoms can be reacted with antimony atoms and formed the orthorhombic Sb_2S_3 (**Figure 1**c). The NSSCs composite can still maintain the 1D nanofiber structure after the heat-treatment as shown in the insert of **Figure 1**c. The overall reaction processes could be expressed as follows.

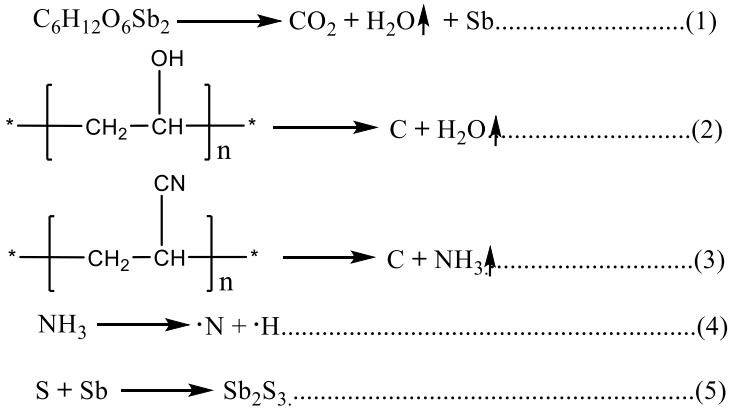

The crystal textures of as-prepared sample are shown in **Figure 1**d. All the diffraction peaks are satisfactorily ascribed to the orthorhombic Sb_2S_3 (JCPDS File No. 42-1293) after sulfuration in a sealed quartz tube. No impure peaks are detected and the crystallinity can reach to 95.8% after a refine evaluation, demonstrating that NSSCs material with superior fineness, which can be prepared via the efficient electrospun. Furthermore, carbon material structure is certified by the Raman spectra. As shown in, The disorder-induced feature (D bands) and the E2g patterns of graphite (G bands) can be observed, and they located at 1363 and 1583 cm^{-1}, respectively (**Figure S1**, **Supporting Information**).[39] The X-ray photoelectron spectroscopy (XPS) spectra is further used to elucidate the valence-bond of the sample (**Figure 1**). The peaks of N 1*s* locate at 397.8, 399.9 and 401.6 eV are allotted to the pyridinic-N, pyrrolic-N and

graphitic-N, respectively.[23] The N-doping carbon nanofibers can afford plentiful electrons to advance the electronic conductivity of the carbon nanofiber and advance the Li-storage performance. The Sb 4d spectrum shows three major peaks, located at 35.1, 33.8 and 32.2 eV, respectively, corresponding to Sb $4d_{3/2}$, $4d_{5/2}$ and $4d$, which can be attributed to the Sb (III) in NSSCs (**Figure S2**a, **Supporting Information**). The binding energy of $2p_{1/2}$ and $2p_{3/2}$ of S (II) are located at 163.6 and 162.5 eV, respectively, (**Figure S2**b, **Supporting Information**). All the results successfully demonstrate that the annealing carbonization and sulfuration processes are absolute. Moreover, the structure and purity of the final product are compelling.[40]

Because of the high boiling point and nonvolatile for antimony, the facts of zero discharge and high atom utilization for nitrogen, sulfur and antimony elements are confirmed by precise assessment of the atom percent in the precursor and final product. The atom percent of N, S and Sb are 2.67%, 58.41% and 38.93% in the precursor, respectively. According to the Energy Dispersive X-Ray Spectroscopy (EDX) and XPS spectra (**Figure S3**, **Supporting Information**), the atom percent of N, S and Sb can be calculated to be 2.54%, 27.63% and 69.83% in the final product, respectively. The results are closely consistent with the atom percent in the precursor, which could also verify the N-doping strategy with a one-step annealing is effective and nearly zero nitrogen discharge. Moreover, the Sb_2S_3 nanoparticle content in the composite is deduced by TG-DSC as shown in **Figure 1**f. Two obvious exothermic peaks at both 461 °C and 537 °C, which could be assigned to the burning process of carbon matrix and Sb_2S_3 nanoparticles, respectively. The final oxidation product is Sb_2O_3 and its

weight percentage is 11.36%, which can speculate that the atomic ratio of S and Sb is 3:2. This result further confirms the form of S and Sb elements in carbon fibers. Meanwhile, the Sb_2S_3 nanoparticle in the carbon nanofibers is 49.06% on account of the mass loss from carbon matrix.

The N-doped Sb_2S_3 carbon fibers were attained by an electrospinning method, as illustrated in **Figure 2**a. The dimension of precursor nanofiber exceeds 30 μm, providing a self-supporting interpenetrating network (**Figure S4**a-b, **Supporting Information**). The fibers shrunk for the follow-up annealing process with a decrease size of 70 nm (**Figure 2**b and **Figure S4**c, **Supporting Information**). Additionally, the product can still maintain fiber structure and its surface is smooth with few particles after the sulfuration process. The average diameter of NSSCs is about 200 nm (**Fig. S4**d, **Supporting Information**). Moreover, the elements of C, N, S and Sb can be distinguished in the **Figure 2**c. The nanoscale active material can provide large specific area and more action sites. The as-prepared NSSCs composite endows an advanced interlinked 3D conductive network, which successfully constructed a binder-free and flexible electrode. Consequently, the interactions between NSSCs anode and electrolyte are reinforced, which may strengthen its cycle and rate performance in the LIBs. **Figure 2**d is enlarged area as indicated by the arrows (yellow box) in **Figure S5**a (**Supporting Information**), respectively. The Sb_2S_3 nanoparticles are homogenously situated in carbon nanofiber matrix and the distribution of particle size are shown in **Figure S5**b-c (**Supporting Information**), which can speculate the size of Sb_2S_3 nanoparticle is about 15 nm. The high-resolution transmission electron microscopy (HRTEM) image

displays a d-spacing of 0.317 nm for parallel fringes, which are consistent with the crystal (021) plane of orthorhombic Sb_2S_3 (**Figure S5**d, **Supporting Information**). Meanwhile, the selected area electron diffraction (SAED) pattern can be well assigned to the pure Sb_2S_3 phase, consistent with the diffraction peaks of (021), (130) and (002) planes revealed in the XRD pattern (**Figure 2**e). **Figure 2**f reveals the elemental distribution in the NSSCs composite by HAADF-STEM. Carbon, sulfur, antimony and nitrogen are identified in the fibers and the component of S and Sb is located in the carbon matrix. The 3D interconnected network offers rapid electrical channels and the surrounding amorphous carbon matrix structure also plays a durable buffer unit to assuage the volume expansion stress during the charge-discharge process.

The binder-free and flexible films of NSSCs composite are straight used as electrode for LIBs. Its electrochemical performance of NSSCs is studied by CR2032 coin-type cells using Li-metal as the counter electrode for LIBs. The cyclic voltammetry (CV) curves of the NSSCs anode between 0.01 V and 3.00 V as shown in **Figure 3**a. Two distinct cathodic peaks locate at 1.32 and 0.76 V, and a broad peak locates at 0.23 V, which can be ascribed to the multistep reactions including the disintegration of electrolyte and the formation of a SEI layer during the first cathode scan.[41, 42] Two anodic peaks at 1.09 and 2.34 V can be accredited to dealloy and conversation process, respectively. All the facts can confirm the hierarchical electrochemical reactions of the NSSCs anode, which are in accord with the reported Sb_2S_3 anode materials.[21, 22, 43] The total discharge-charge process of the NSSCs anode are stated using the following equations:

Discharge:

$$Sb_2S_3 + 6Li^+ + 6e^- \xrightarrow{1.32\ V} 3Li_2S + 2Sb \quad (5)$$

$$Sb + 3Li^+ + 3e^- \xrightarrow{0.76\ V} Li_3Sb \quad (6)$$

Charge:

$$Li_3Sb - 3e^- \xrightarrow{1.09\ V} Sb + 3Li^+ \quad (7)$$

$$2Sb + 3Li_2S - 6e^- \xrightarrow{2.34\ V} Sb_2S_3 + 6Li^+ \quad (8)$$

The charge-discharge curves of the NSSCs electrode at a specific current density with a value of 1 A g^{-1} is shown in **Figure 3**b. The initial discharge-charge capacities of NSSCs electrode are 1110 mA h g^{-1} and 780 mA h g^{-1}, respectively. And its initial Coulombic Efficiency (CE) is 70%. The first cycle delivering irreversible capacity are mainly ascribed to the establishment of the SEI film and electrochemical disintegration of the solvent in the cell. It is worthy of a lot of pyrolyzed carbon from the PAN precursor will reduce the initial CE and electrochemical properties of the NSSCs anode. And the pyrolyzed carbon at 700 °C can only carry a capacity of 70 mA h g^{-1} at 0.2 A g^{-1} after 200 cycles with 61.3% initial CE (**Figure S6**, **Supporting Information**). The capacity donated by NSSCs electrode is about 606.3 mA h g^{-1} after 150 cycles and deliver a superior capacity retention (83%). The CE of the second cycle is close to 100% and keeps unchanging for the rest 150 cycles.

High cycle performance is a critical factor for battery-operated applications. The NSSCs anode shows unchanging cycle performances at 0.2 A g^{-1} with a good initial discharge capacity of 1110 mA h g^{-1} and a finished capacity of 606.3 mA h g^{-1} after 150 cycles (**Figure 3**d). Even at 1 A g^{-1}, the NSSCs electrode can still deliver a high capacity of 490.3 mA h g^{-1} after the long-time cycles (**Figure 3**e). For comparison, the undoped

Sb_2S_3 carbon fibers (SSCs) and ordinary Sb_2S_3 particles (SSPs) electrodes only can obtain a capacity of 443.3 and 93.1 mA h g^{-1} after 150 cycles, respectively because of their poor conductivity and uncontrolled volume variation throughout the charge-discharge process (**Figure S7**a, **Supporting Information**). Furthermore, the cycled morphology indicates that the SSPs cluster together and partial particles are cracked (**Figure S7**b, **Supporting Information**). The rate properties of the NSSCs anode is revealed in **Figure 3**c. As the cyclic capacity keep unchanging after 20 cycles, therefore, the rate performance was steered after pre-cycling 20 cycles at 0.2 A g^{-1}. The discharge capacity only slightly drops from 0.2 A g^{-1} to 8 A g^{-1}. Once the current density reaches to 0.2, 1, 4 and 8 A g^{-1}, the release capacities are 657, 631, 483 and 336 mA h g^{-1}, respectively. And the current densities were set back to 0.2 A g^{-1}, the reversible capacity can be regained to 603 mA h g^{-1} exhibiting outstanding rate performance. The outcomes show that the NSSCs electrode demonstrates more advanced reversible capacity and cycling properties than other reported Sb_2S_3 anode materials (**Table S1**, **Supporting Information**).

To bring real impact and commercialize the NSSCs as a promising anode material, the full cell performance is very critical. The full cell is assembled by coupling α-$NaFeO_2$ Al_2O_3-$LiNi_{0.8}Co_{0.15}Al_{0.05}O_2$ cathode (AO-NCA) with the as-developed NSSCs anode.[44] The nickel-rich cathode has been wildly used in energy storage devices due to its high theoretic capacity, stable charge-discharge plateau and low price. The NSSCs anode are authorized to achieve twelve electrons, and the AO-NCA cathode principally holds twelve Li-ions extraction ability. The integral chemical reaction of the battery is

revealed as follows:

$$LiNi_{0.8}Co_{0.15}Al_{0.05}O_2 + Sb_2S_3 \underset{}{\overset{12*(0.8-x)e^-}{\rightleftharpoons}} Li_{0.2+x}Ni_{0.8-x}Co_{0.15}Al_{0.05}O_2 + Li_3Sb + Li_2S \quad (9)$$

For safety design of the full cell, the anode capacity is excess 15% than that of AO-NCA cathode. Moreover, the charge-discharge voltage is restricted between 3.0 and 4.2 V to assure the layered structure stability of NCO cathode and the safe operation of the full cell. The assembled cell packages were refolded 300 times before electrochemistry performance test and the Li-storage property of the battery is evaluated as exhibited in **Figure 4**a-d. The representative charge-discharge profiles of the full cell at a current rate of 0.1 C were shown in **Figure 4**a. The specific capacity of anode material is evaluated on account of the counter electrode mass. The first discharge profile reveals a distinct potential plateau around 3.75 V. The plateau preserves steadily in the succeeding cycles, which is corresponding with the CV curves (**Figure S8**, **Supporting Information**). The initial charge and discharge capacities of the cathode are 234.4 and 194.5 mA h g^{-1}, respectively, with a CE of 82.9%. The charge-discharge profiles almost overlap at following cycles. The rate capability of the cathode is also assessed by applying several kinds of current from 0.5 to 32 C (**Figure 4**b) after 10 pre-cycling. The cathode delivers superior reversible capacities of 187, 163, 129, 106, 83 and 48 mA h g^{-1} at 0.5, 1, 4, 8, 16 and 32 C, respectively. And when the current was set back to 0.5 C, the reversible capacity can be returned to 185 mA h g^{-1}. The value is near to its initial capacity, indicating its good acceptance of large current rate. Effective capacity as high as 177.8 mA h g^{-1} can still be sustained at 0.5 C after 200 cycles, which indicates that the superior long-term cycling performance (**Figure 4**c). It

is worth noting that the NSSCs anode can deliver a capacity of 600 mA h g^{-1} after 200 cycles at the same current density by cathode capacity conversion. As shown in **Figure 4**d-f, the full cell with a charge state can well drive a motor and power on an electronic thermometer. The results verify the NSSCs electrode can well match with cathodic material and show superior Li-storage with a promising potential for portable equipment and power unit.

Benefiting from the well-designed structure and new idea of synthetic route, the NSSCs electrode with improved conductivity and carbon buffer matrix exhibits superior Li-storage performance. The electronic transfer, Li-ions diffusion mechanism and volume expansion were simulated of NSSCs electrode (**Figure 5**). A synergistic effect of high temperature treatment and the abundant fibers forming an enormous electrons transportation channel. As a result, it can provide an expressway for electrons transport leading an excellent electroconductibility of NSSCs electrode (**Figure 5**a). Electrochemical impedance spectroscopy (EIS) is applied to verify the superior Li-ions diffusion and electric conductivity mechanism of NSSCs electrode (**Figure 5**c-d). The equivalent circuit model is shown in the **Supporting note 1**. The internal resistance (R_{ct}) values are 60, 100 and 428 Ω for NSSCs, SSCs and SSPs electrodes, respectively, which illustrate more advanced electric conductivity and worse inferior ions diffusion resistance than undoped Sb_2S_3 carbon fiber a and single component SSPs.[45-47] The "σ" value negatively correlated with the "D" value (**Supporting note 2**) and all the σ values of anodes are displayed in **Figure 5**d.[48] The σ values are 19, 24 and 30 corresponding to NSSCs, SSCs and SSPs anodes, respectively. These results are consensus with the

gradients of the real part "$\omega^{-1/2}$". The results indicate that the N-doping matrix carbon fibers can successfully advance the conductivity and Li-ion diffusion of the NSSCs anode. The controlled-release mechanism of charge-discharge process accompanying the volume expansion is also shown in **Figure 5**b. The Sb_2S_3 nanoparticles imbedded in the matrix carbon fibers constructed a stable protective layer, which can positively confine the volume variation during the Li-ions intercalation course. The exceptional structure can offer a structurally firm parasitifer for Li-ions diffusion process. Noteworthily, the Sb_2S_3 nanoparticles are still embedded in the carbon matrix after long-time cycles. This phenomenon can attest the NSSCs electrode is great steady for high performance LIBs (**Figure S9**a, **Supporting Information**). Moreover, after high-rate cycling, the TEM structure of NSSCs still holds its primary structure without and none of the Sb_2S_3 nanoparticles aggregate. The results can be confirmed by **Figure S9**b (**Supporting Information**). All the results illustrate that the NSSCs 3D interconnected network which is comprised of abundant Sb_2S_3 nanoparticles and carbon nanofibers composites can successfully advance the electric conductivity, Li-ions diffusion and release the volume expansion to ensure the excellent Li-storage for LIBs.

CONCLUSIONS

In summary, we demonstrate an eco-friendly method to synthesize the self-supported N-doped Sb_2S_3 carbon fibers (NSSCs) with high atom utilization and zero discharge for nitrogen and sulfur, by annealing the electrospinning precursor in a sealed quartz tube. The NSSCs electrode with improved conductivity and carbon buffer matrix exhibits excellent electrochemical performance, and it can obtain a capacity of 490.3 mA h g^{-1}

at a current density of 1 A g^{-1} after 1000 cycles. It even sustained a capacity of 600 mA h g^{-1} at a current rate of 0.5 C after 200 cycles for the full cell. The excellent Li-storage performance further reveals that the NSSCs anode has tremendous potential for the energy storage application. In addition, this eco-friendly approach can be widely extended to synthesize various flexible metal sulfides and metal nitrides with high atom utilization and zero discharge.

Experimental section

Materials Synthesis. Synthesis of N-doped Sb_2S_3 carbon nanofibers: 1 g polyvinyl alcohol (PVA, average Mw = 88,000, Sigma-Aldrich), 0.05 g Polyacrylonitrile (PAN, average Mw = 150,000, Sigma-Aldrich), 0.6 g antimony glycolate ($C_6H_{12}O_6Sb_2$, 99%, Sigma-Aldrich) and 0.6 g sulfur powder (99%, Sigma-Aldrich) were liquified in N, N-dimethylformamide (DMF, anhydrous, 99.8%, Aldrich), dimethylacetamide (DMAc, anhydrous, 99.8%, Sigma-Aldrich) and carbon disulfide (CS_2, 99.8%, Sigma-Aldrich) for 12 h with continuous stirring at 65 °C. The precursor solution was placed in a 5 mL with a 23-gauge syringe needle, and then was applied to electrospun on spinning system (TEADFS-100, BJ TECHNOVA) at 19 kV. An aluminum foil located 15 cm away from the needle was utilized to collect the film at a speed of 20 rpm min^{-1}. The whole synthesis process was carried out in an airtight box (humidity below 40%). The obtained films were cut into small squares (1.5*1.5 cm) and placed into a vacuum quartz tube. The first heat-treatment was set at 5 °C min^{-1} up to 280 °C for 4 h for stabilizing the fiber structure. The temperature further increased to 700 °C for carbothermal and sulfuration reaction. Then, the furnace temperature decreased to

450 °C for 2 h to stabilize the final product. Lastly, the obtained NSSCs electrode was dried in a vacuum oven to remove the residual moisture at 80 °C.

Synthesis of Sb_2S_3 nanoparticles. The stoichiometry of antimony powder and sulfur powder were placed in a laboratory planetary mill (QM-3SP04, Nanjing, China) and the speed was controlled at 400 rpm min^{-1}. And the Sb_2S_3 nanoparticles can be obtained after milling for 12 h.[49]

Preparation of Al_2O_3 coated $LiNi_{0.8}Co_{0.15}Al_{0.05}O_2$: Stoichiometric amount of reactants $Al_3(NO_3)_2 \cdot 9H_2O$ (AR, 99%), $Ni(CH_3COO)_2 \cdot 4H_2O$ (AR, 99%), $Co(CH_3COO)_2 \cdot 4H_2O$ (AR, 99%) and $CH_3COOLi \cdot 2H_2O$ were dissolved in deionized water. Citric acid was added with the equal molar ratio of the total transition metal ions. Then ammonium hydroxide solution was used to adjust the precursor pH and the value was maintained at 6.7. The obtained gel was transferred into a vacuum oven and dried at 120 °C for 12 h, forming the amorphous powders. The as-prepared powder was disposed at 500 °C for 5 h to take away the organic component and then calcined at 700 °C for 10 h to obtain the final product.[44, 50] Then, 100 mg $LiNi_{0.8}Co_{0.15}Al_{0.05}O_2$ powder was dispersed in DMF and 15 mg aluminum isopropoxide (AR, 99%) was added in the mixed liquor for continuous stirring with 3 h . Lastly, the compound was desiccated in an oven at 150 °C for 10 h, and calcinated at 400 °C to form Al_2O_3 coated $LiNi_{0.8}Co_{0.15}Zn_{0.05}O_2$ cathode material (AO-NCA).

Material Characterization. The scanning electron microscopy (SEM, NOVA 450, FEI) and a transmission electron microscopy (TEM, G2, F30 FEI) were used to obtain morphology of the NSSCs before and after charge-discharge cycles, respectively. The

X-ray diffraction (x'pert3 powder) was used to characterized the crystalline structures of the as-prepared nanofibers. Raman spectra of the products were performed on a Thermo scientific FT-Raman spectrometer (FRA 106/s) with an excitation wavelength of 532 nm. The TG measurement (Diamond TGA/DSC 6300) at a heating rate of 5 ℃ min^{-1} in air and N_2 was used to analysis the composition of NSSCs. X-ray electron spectrometer (XPS, AXIS-ULTRA DLD-600W) was used to analysis the valence states of NSSCs.

Electrochemical Measurements. The NSSCs and SSCs films were directly used as electrode with a dimension of 10 mm. And then the electrode material (80 wt%), acetylene black (10 wt%) and binder (10 wt% polyvinylidene fluoride, PVDF) are mixed in solvent for the preparation of SSPs anode sheets. The mass of the active material was maintained at 2.7 mg cm^{-2}. Moreover, the thickness of anode is around 0.30 mm. The batteries were packaged with lithium foil, electrolyte and separator in a glove box with ultralow water/oxygen values. The full cells were packaged by coupling with Al_2O_3-$LiNi_{0.8}Co_{0.15}Al_{0.05}O_2$ cathode. The LAND cycler (CT 2001, Wuhan Kingnuo Electronic Co., China) was used to conduct the galvanostatic charge-discharge and the CHI 760D electrochemical workstation (ChenHua Instruments Co., China) were used to carry out cyclic voltammetric and electrochemical impedance spectroscopy.

ASSOCIATED CONTENT

Supporting Information

The Supporting Information is available free of charge at:
Raman spectra, XPS spectra, element **quantitative analysis**, SEM images, TEM

images, Cycling performance, voltammetric analysis, EIS analysis.

AUTHOR INFORMATION

***Corresponding Author**

E-mail: xwlv@ctgu.edu.cn (X. L.);

E-mail: bizhui@um.edu.mo (K.N.H.);

E-mail: jun.chen@ucla.edu (J. C.).

Notes

The authors declare no competing financial interest.

Author Contributions

J.C., X.L. and K.N.H. guided the whole project. H.Y., J.C., X.L. and K.N.H. conceived the idea, designed the experiment, analyzed the data, drew the figures, and composed the manuscript. All authors made technical comments on the manuscript. J.C. submitted the manuscript and was the lead contact.

ACKNOWLEDGMENT

J. C. acknowledged the Henry Samueli School of Engineering & Applied Science and the Department of Bioengineering at University of California, Los Angeles for the startup support. X. L acknowledged the National Natural Science Foundation of China (No. 21902084). K. N. H acknowledged the Science and Technology Development Fund, Macau SAR (File no. 191/2017/A3, 041/2019/A1, 046/2019/AFJ), the Multi-Year Research Grants (MYRG2017-00216-FST and MYRG2018-00192-IAPME) from the Research Services and Knowledge Transfer Office at the University of Macau, and the UEA funding.

REFERENCES

1. Xia, C.; Kwok, C. Y.; Nazar, L. F., A high-energy-density lithium-oxygen battery based on a reversible four-electron conversion to lithium oxide. *Science* **2018,** *361* (6404), 777-781.

2. Wan, J.; Xie, J.; Kong, X.; Liu, Z.; Liu, K.; Shi, F.; Pei, A.; Chen, H.; Chen, W.; Chen, J.; Zhang, X.; Zong, L.; Wang, J.; Chen, L. Q.; Qin, J.; Cui, Y., Ultrathin, flexible, solid polymer composite electrolyte enabled with aligned nanoporous host for lithium batteries. *Nat. Nanotechnol.* **2019,** *14* (7), 705-711.

3. Yin, H.; Shen, W.; Qu, H.-Q.; Li, C.; Zhu, M.-Q., Boosted charge transfer and Na-ion diffusion in cooling-fins-like Sb_2Te_3-Te nano-heterostructure for long cycle life and high rate capability anode. *Nano Energy* **2020,** *70*, 104468.

4. Service, R. F., Lithium-ion battery development takes Nobel. *Science* **2019,** *366* (6463), 292-292.

5. Xia, J.; Liu, L.; Jamil, S.; Xie, J.; Yan, H.; Yuan, Y.; Zhang, Y.; Nie, S.; Pan, J.; Wang, X., Free-standing SnS/C nanofiber anodes for ultralong cycle-life lithium-ion batteries and sodium-ion batteries. *Energy Storage Mater.* **2019,** *17*, 1-11.

6. Zheng, J. X.; Zhao, Q.; Tang, T.; Yin, J. F.; Quilty, C. D.; Renderos, G. D.; Liu, X. T.; Deng, Y.; Wang, L.; Bock, D. C.; Jaye, C.; Zhang, D. H.; Takeuchi, E. S.; Takeuchi, K. J.; Marschilok, A. C.; Archer, L. A. Reversible epitaxial electrodeposition of metals in battery anodes. *Science* **2019,** *366* (6465), 645.

7. Xu, S.; Liang, X.; Wu, X., Zhao, S., Chen, J., Wang, K., Chen, J. Multistaged discharge constructing heterostructure with enhanced solid-solution behavior for long-life lithium-oxygen batteries. *Nat. Commun.* **2020,** *10*, 5810.

8. Liu, K.; Kong, B.; Liu, W.; Sun, Y. M.; Song, M. S.; Chen, J.; Liu, Y. Y.; Lin, D. C.; Pei, A.; Cui, Y., Stretchable Lithium Metal Anode with Improved Mechanical and Electrochemical Cycling Stability. *Joule* **2018,** *2* (9), 1857-1865.

9. Makaremi, M.; Mortazavi, B.; Singh, C. V., Carbon ene-yne graphyne monolayer as an outstanding anode material for Li/Na ion batteries. *Appl. Mater. Today* **2018,** *10*, 115-121.

10. Cerdán-Pasarán, A.; López-Luke, T.; Mathew, X.; Mathews, N. R., Effect of cobalt doping on the device properties of Sb_2S_3-sensitized TiO_2 solar cells. *Solar Energy* **2019,** *183*, 697-703.

11. Li, F.; Zhang, L.; Hu, C.; Xing, X.; Yan, B.; Gao, Y.; Zhou, L., Enhanced azo dye decolorization through charge transmission by σ-Sb^{3+}-azo complexes on amorphous Sb_2S_3 under visible light irradiation. *Appl. Catal. B-Environ.* **2019,** *240*, 132-140.

12. Li, Z.; Lin, C.; Qu, G.; Calvez, L.; Dai, S.; Zhang, X.; Xu, T.; Nie, Q., Formation and properties of chalcogenide glasses based on GeS_2-Sb_2S_3-AgI system. *Mater. Lett.* **2014,** *132*, 203-205.

13. Xie, F.; Zhang, L.; Gu, Q.; Chao, D.; Jaroniec, M.; Qiao, S.-Z., Multi-shell hollow structured Sb_2S_3 for sodium-ion batteries with enhanced energy density. *Nano Energy* **2019,** *60*, 591-599.

14. Xie, J.; Liu, L.; Xia, J.; Zhang, Y.; Li, M.; Ouyang, Y.; Nie, S.; Wang, X., Template-free synthesis of Sb_2S_3 hollow microspheres as anode materials for lithium-ion and sodium-ion batteries. *Nano-micro letters* **2018,** *10* (1), 12.

15. Wu, X. H.; Pan, K. C.; Jia, M. M.; Ren, Y. F.; He, H. Y.; Zhang, L.; Zhang, S. J.,

Electrolyte for lithium protection: From liquid to solid. *Green Energy Environ.* **2019,** *4* (4), 360-374.

16. Yin, H.; Liu, Y.; Yu, N.; Qu, H.-Q.; Liu, Z.; Jiang, R.; Li, C.; Zhu, M.-Q., Graphene-like MoS_2 nanosheets on carbon fabrics as high-performance binder-free electrodes for supercapacitors and Li-ion batteries. *ACS Omega* **2018,** *3* (12), 17466-17473.

17. Yu, X.-X.; Wang, L.; Yin, H., Hierarchical heterojunction structures based-on layered Sb_2Te_3 nanoplate@rGO for extended long-term life and high-rate capability of sodium batteries. *Appl. Mater. Today* **2019,** *15*, 582-589.

18. Tian, H.; Liu, H.; Yang, T. Y.; Veder, J. P.; Wang, G. X.; Hu, M.; Wang, S. B.; Jaroniec, M.; Liu, J., Fabrication of core-shell, yolk-shell and hollow Fe_3O_4@carbon microboxes for high-performance lithium-ion batteries. *Mater. Chem. Front.* **2017,** *1* (5), 823-830.

19. Pomerantseva, E.; Bonaccorso, F.; Feng, X. L.; Cui, Y.; Gogotsi, Y., Energy storage: The future enabled by nanomaterials. *Science* **2019,** *366* (6468), 969.

20. Li, C.; Song, H.; Mao, C.; Peng, H.; Li, G., A novel MoS_2 nanosheets-decorated Sb@Sb_2S_3@C tubular composites as anode material for high performance lithium ion battery. *J. Alloy. Compd.* **2019,** *786*, 169-176.

21. Yi, Z.; Han, Q.; Cheng, Y.; Wu, Y.; Wang, L., Facile synthesis of symmetric bundle-like Sb_2S_3 micron-structures and their application in lithium-ion battery anodes. *Chem. Commun.* **2016,** *52* (49), 7691-7694.

22. Luo, W.; Ao, X.; Li, Z.; Lv, L.; Li, J.; Hong, G.; Wu, Q.-H.; Wang, C., Imbedding ultrafine Sb_2S_3 nanoparticles in mesoporous carbon sphere for high-performance

lithium-ion battery. *Electrochim. Acta* **2018,** *290*, 185-192.

23. Xie, J.; Xia, J.; Yuan, Y.; Liu, L.; Zhang, Y.; Nie, S.; Yan, H.; Wang, X., Sb_2S_3 embedded in carbon-silicon oxide nanofibers as high-performance anode materials for lithium-ion and sodium-ion batteries. *J. Power Sources* **2019,** *435*, 226762.

24. Bag, S.; Roy, A.; Mitra, S., Sulfur, Nitrogen Dual Doped Reduced Graphene Oxide Supported Two-Dimensional Sb_2S_3 Nanostructures for the Anode Material of Sodium-Ion Battery. *ChemistrySelect* **2019,** *4* (22), 6679-6686.

25. Li, M.; Huang, F.; Pan, J.; Li, L.; Zhang, Y.; Yao, Q.; Zhou, H.; Deng, J., Amorphous Sb_2S_3 Nanospheres In-Situ Grown on Carbon Nanotubes: Anodes for NIBs and KIBs. *Nanomaterials* **2019,** *9* (9), 1323.

26. Luo, W.; Li, F.; Zhang, W.; Han, K.; Gaumet, J.-J.; Schaefer, H.-E.; Mai, L., Encapsulating segment-like antimony nanorod in hollow carbon tube as long-lifespan, high-rate anodes for rechargeable K-ion batteries. *Nano Res.* **2019,** *12* (5), 1025-1031.

27. Yin, H.; Qu, H.-Q.; Liu, Z.; Jiang, R.-Z.; Li, C.; Zhu, M.-Q., Long cycle life and high rate capability of three dimensional $CoSe_2$ grain-attached carbon nanofibers for flexible sodium-ion batteries. *Nano Energy* **2019,** *58*, 715-723.

28. Zhou, Z.; Padgett, S.; Cai, Z.; Conta, G.; Wu, Y.; He, Q.; Zhang, S.; Sun, C.; Liu, J.; Fan, E.; Meng, K.; Lin, Z.; Uy, C.; Yang, J.; Chen, J. Single-layered ultra-soft washable smart textiles for all-around ballistocardiograph, respiration, and posture monitoring during sleep. *Biosens. Bioelectron.* **2020**, *155*,112064.

29. Chen, J.; Huang, Y.; Zhang, N.; Zou, H.; Liu, R.; Tao, C.; Fan, X.; Wang, Z. L., Micro-cable structured textile for simultaneously harvesting solar and mechanical

energy. *Nat. Energy* **2016,** *1* (10), 16138.

30. Chen, J.; Wang, Z. L., Reviving vibration energy harvesting and self-powered sensing by a triboelectric nanogenerator. *Joule* **2017,** *1* (3), 480-521.

31. Yan, C.; Gao, Y.; Zhao, S.; Zhang, S.; Zhou, Y.; Deng, W.; Li, Z.; Jiang, G.; Jin, L.; Tian, G., Yang, T., Chu, X., Xiong, D., Wang, Z., Li, Y., Yang, W., Chen, J. A linear-to-rotary hybrid nanogenerator for high-performance wearable biomechanical energy harvesting. *Nano Energy* **2020,** *67*, 104235.

32. Zhou, Z.; Chen, K.; Li, X.; Zhang, S.; Wu, Y.; Zhou,Y.; Meng, K.; Sun, C.; He, Q.; Fan, W.; Fan, E.; Lin, Z.; Tan, X.; Deng, W.; Yang, J.; Chen, J. Sign-to-speech translation using machine-learning-assisted stretchable sensor arrays. *Nat. Electron.* **2020**, *3* , 430.

33. Meng, K.; Zhao, S.; Zhou, Y.; Wu, Y.; Zhang, S.; He, Q.; Wang, X.; Zhou, Z.; Fan, W.; Tan, X., A Wireless Textile Based Sensor System for Self-Powered Personalized Health Care. *Matter* **2019,** *2* (4), 896-907.

34. N. Zhang; F. Huang; S. Zhao; X. Lv; Y. Zhou; S. Xiang; S. Xu; Y. Li; G. Chen; C. Tao; Y. Nie; J. Chen; Fan, X., Photo-rechargeable fabrics as sustainable and robust power sources for on-body electronics. *Matter* **2020,** *2* (5), 1260-1269.

35. Chen, G.; Li, Y.; Bick, M.; Chen, J. Smart textiles for electricity generation. *Chem. Rev.* **2020**, *120* (8), 3668-3720.

36. Gong, W.-L.; Xiong, Z.-J.; Xin, B.; Yin, H.; Duan, J.-S.; Yan, J.; Chen, T.; Hua, Q.-X.; Hu, B.; Huang, Z.-L., Twofold photoswitching of NIR fluorescence and EPR based on the PMI-N-HABI for optical nanoimaging of electrospun polymer nanowires. *J.*

Mater. Chem. C **2016,** *4* (13), 2498-2505.

37. Yin, H.; Cao, M.-L.; Yu, X.-X.; Zhao, H.; Shen, Y.; Li, C.; Zhu, M.-Q., Self-standing Bi_2O_3 nanoparticles/carbon nanofiber hybrid films as a binder-free anode for flexible sodium-ion batteries. *Mater. Chem. Front.* **2017,** *1* (8), 1615-1621.

38. Yin, H.; Li, Q.; Cao, M.; Zhang, W.; Zhao, H.; Li, C.; Huo, K.; Zhu, M., Nanosized-bismuth-embedded 1D carbon nanofibers as high-performance anodes for lithium-ion and sodium-ion batteries. *Nano Res.* **2017,** *10* (6), 2156-2167.

39. Cao, X. M.; Sun, Z. J.; Zhao, S. Y.; Wang, B.; Han, Z. B., MOF-derived sponge-like hierarchical porous carbon for flexible all-solid-state supercapacitors. *Mater. Chem. Front.* **2018,** *2* (9), 1692-1699.

40. Reiser, P.; Benneckendorf, F. S.; Barf, M. M.; Muller, L.; Bauerle, R.; Hillebrandt, S.; Beck, S.; Lovrincic, R.; Mankel, E.; Freudenberg, J.; Jansch, D.; Kowalsky, W.; Pucci, A.; Jaegermann, W.; Bunz, U. H. F.; Mullen, K., n-Type Doping of Organic Semiconductors: Immobilization via Covalent Anchoring. *Chem. Mater.* **2019,** *31* (11), 4213-4221.

41. Jing, L. Y.; Lian, G.; Wang, J. R.; Zhao, M. W.; Liu, X. Z.; Wang, Q. L.; Cui, D. L.; Wong, C. P., Porous-hollow nanorods constructed from alternate intercalation of carbon and MoS_2 monolayers for lithium and sodium storage. *Nano Res.* **2019,** *12* (8), 1912-1920.

42. Li, Z. H.; Feng, X. M.; Mi, L. W.; Zheng, J. Y.; Chen, X. Y.; Chen, W. H., Hierarchical porous onion-shaped $LiMn_2O_4$ as ultrahigh-rate cathode material for lithium ion batteries. *Nano Res.* **2018,** *11* (8), 4038-4048.

43. Prikhodchenko, P. V.; Gun, J.; Sladkevich, S.; Mikhaylov, A. A.; Lev, O.; Tay, Y. Y.; Batabyal, S. K.; Yu, D. Y. W., Conversion of Hydroperoxoantimonate Coated Graphenes to Sb_2S_3@Graphene for a Superior Lithium Battery Anode. *Chem. Mater.* **2012,** *24* (24), 4750-4757.

44. Yin, H.; Yu, X.-X.; Zhao, H.; Li, C.; Zhu, M.-Q., Towards high-performance cathode materials for lithium-ion batteries: Al_2O_3-coated $LiNi_{0.8}Co_{0.15}Zn_{0.05}O_2$. *J. Solid State Electr.* **2018,** *22* (8), 2395-2403.

45. Chu, J.; Yu, Q.; Yang, D.; Xing, L.; Lao, C.-Y.; Wang, M.; Han, K.; Liu, Z.; Zhang, L.; Du, W.; Xi, K.; Bao, Y.; Wang, W., Thickness-control of ultrathin bimetallic Fe-Mo selenide@N-doped carbon core/shell "nano-crisps" for high-performance potassium-ion batteries. *Appl. Mater. Today* **2018,** *13*, 344-351.

46. Sun, M.; Zou, L.; Wang, Z.; Guo, S.; Chen, Y.; Chi, B.; Pu, J.; Li, J., Porous nanocubes $La_{0.9}Co_{0.8}Ni_{0.2}O_{3-x}$ as efficient catalyst for Li-O_2 batteries. *Electrochim. Acta* **2019,** *327*, 135017.

47. Nguyen, T. T. M.; Le, H. M.; Kawazoe, Y.; Nguyen, H. L., Reticular control of interpenetration in a complex metal-organic framework. *Mater. Chem. Front.* **2018,** *2* (11), 2063-2069.

48. Ge, P.; Zhang, C.; Hou, H.; Wu, B.; Zhou, L.; Li, S.; Wu, T.; Hu, J.; Mai, L.; Ji, X., Anions induced evolution of Co_3X_4 (X= O, S, Se) as sodium-ion anodes: The influences of electronic structure, morphology, electrochemical property. *Nano Energy* **2018,** *48*, 617-629.

49. Dutková, E.; Takacs, L.; Sayagués, M. J.; Baláž, P.; Kováč, J.; Šatka, A.,

Mechanochemical synthesis of Sb_2S_3 and Bi_2S_3 nanoparticles. *Chem Eng Sci.* **2013,** *85*, 25-29.

50. Zhao, X.; Yu, R.; Tang, H.; Mao, D.; Qi, J.; Wang, B.; Zhang, Y.; Zhao, H.; Hu, W.; Wang, D., Formation of Septuple-Shelled $(Co_{2/3}Mn_{1/3})(Co_{5/6}Mn_{1/6})_2O_4$ Hollow Spheres as Electrode Material for Alkaline Rechargeable Battery. *Adv. Mater.* **2017,** *29* (34), 1700550.

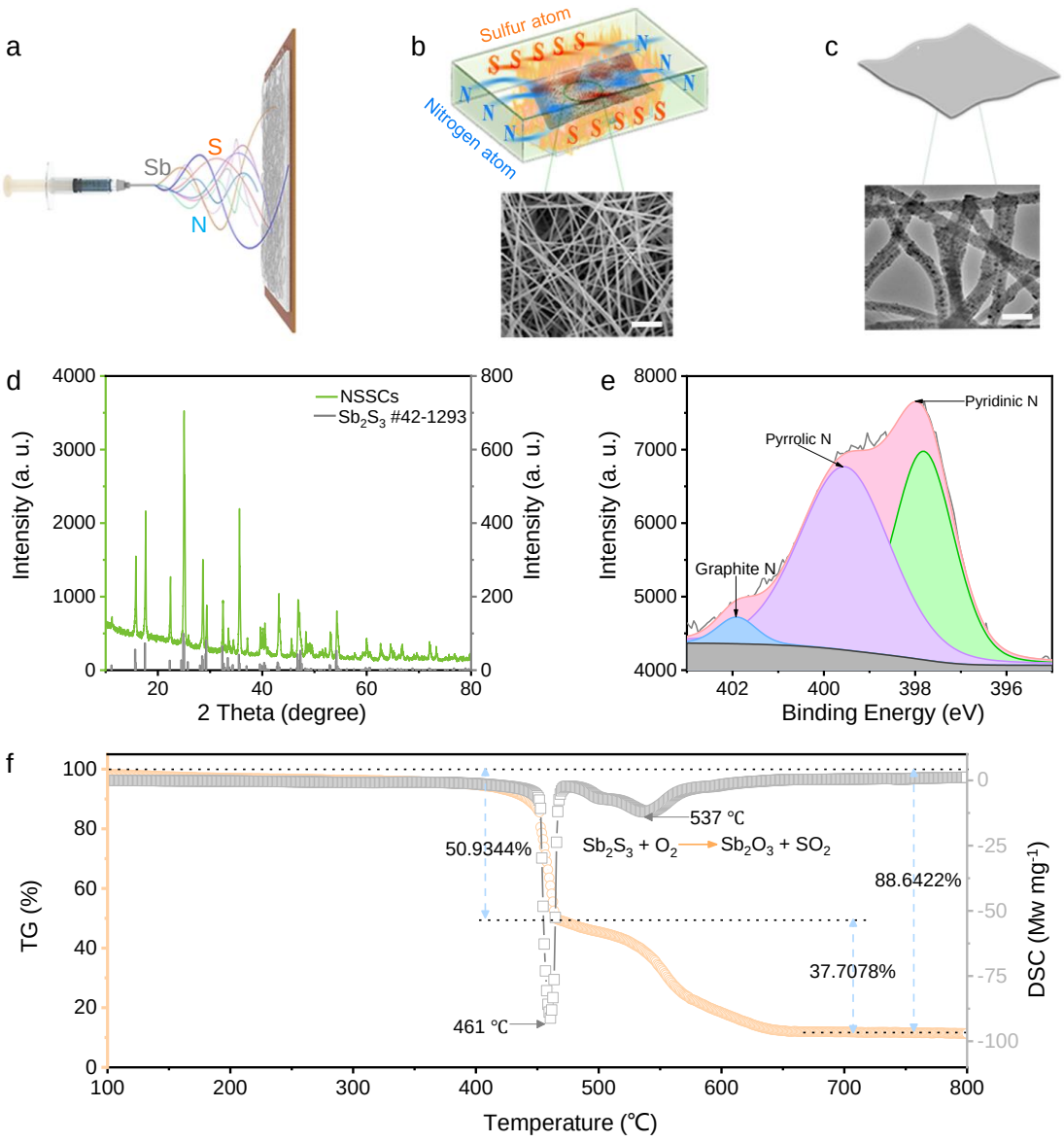

Figure 1. Schematic illustration of the fabrication process and structure of N-doped Sb_2S_3 carbon fibers composite. (a), The electrospinning process. (b), The heat-treatment process and the structure of the electrospun fiber (scale bar, 5 μm). (c), The as-developed NSSCs composite (scale bar, 200 nm). (d), XRD pattern of NSSCs composite. (e), High-resolution XPS spectra of N 1*s*. (f), The TG-DSC curves of NSSCs composite at a heating rate of 5 ℃ min^{-1} in air.

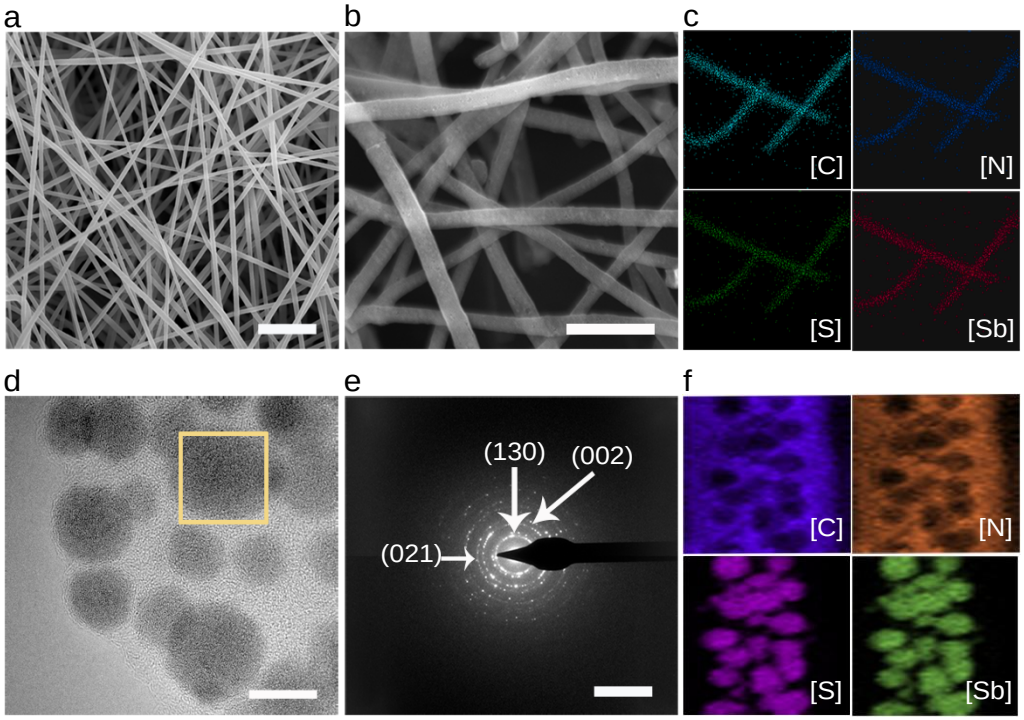

Figure 2. Microstructure characterization of the as-prepared N-doped Sb_2S_3 carbon fibers. (a), SEM image of the precursor fibers (scale bar, 5 μm). (b), SEM image of NSSCs (scale bar, 1 μm). (c), SEM elemental mapping images of C, N, S and Sb elements in the NSSCs composite. (d), TEM image of NSSCs nanofiber (scale bar, 10 nm). (e), The SAED pattern of NSSCs (scale bar, 10.0 1/Gm). (f), TEM HAADF elemental mapping images of C, N, S and Sb elements in the NSSCs composite.

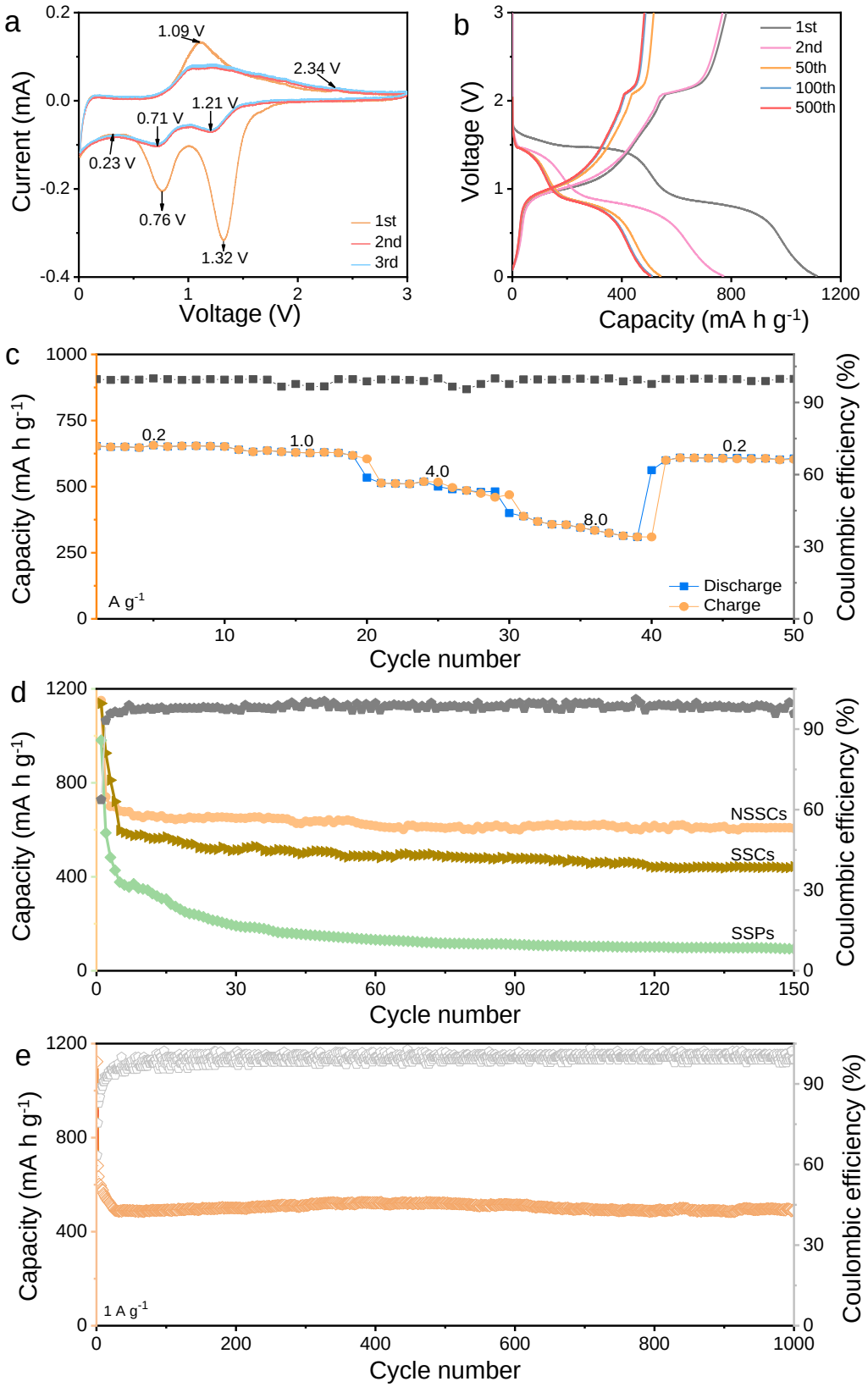

Figure 3. Electrochemical behavior of as-prepared N-doped Sb_2S_3 carbon fibers composite for Li-storage. (a), CV curves of the NSSCs electrode from 0.01 V to 3.0

V at a scan rate of 0.1 mV s^{-1}. (b), The initial discharge-charge profiles of the NSSCs electrode between 0.01 V and 3.0 V at a current rate of 1 A g^{-1}. (c), Cycling performance of the NSSCs, SSCs and SSPs electrodes at a current density of 0.2 A g^{-1}, respectively, and the Coulombic efficiency of NSSCs anode. (d), Rate capability of the NSSCs electrode at various current rates from 0.1A g^{-1} to 8 A g^{-1}. (e), Long-term cycling performance of NSSCs electrode at a cycling rate of 1 A g^{-1} with 1000 cycles.

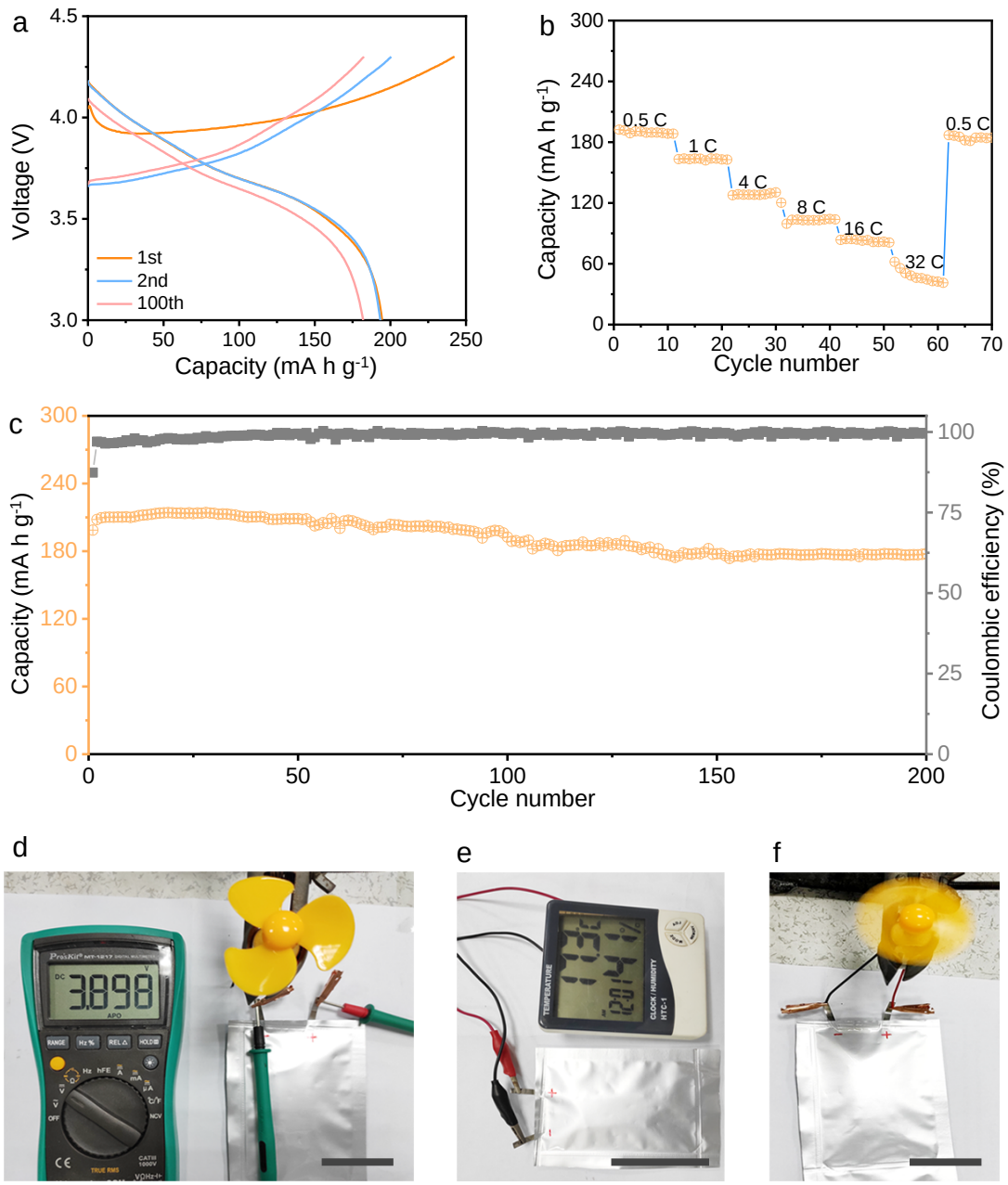

Figure 4. Full battery performance coupled NSSCs anode with AO-NCA cathode. (a), Charge-discharge profiles between 3.0 and 4.2 V. (b), Rate performance with current rate from 0.5 C to 32 C. (c), Cycling performance at a current rate of 0.5 C. (d), The voltage testing of AO-NCA/NSSCs full cell with a charge state (scale bar, 3cm). (e), Driving a motor by the full cell (scale bar, 3cm). (f), Lighting an electronic thermometer by the full cell (scale bar, 5cm).

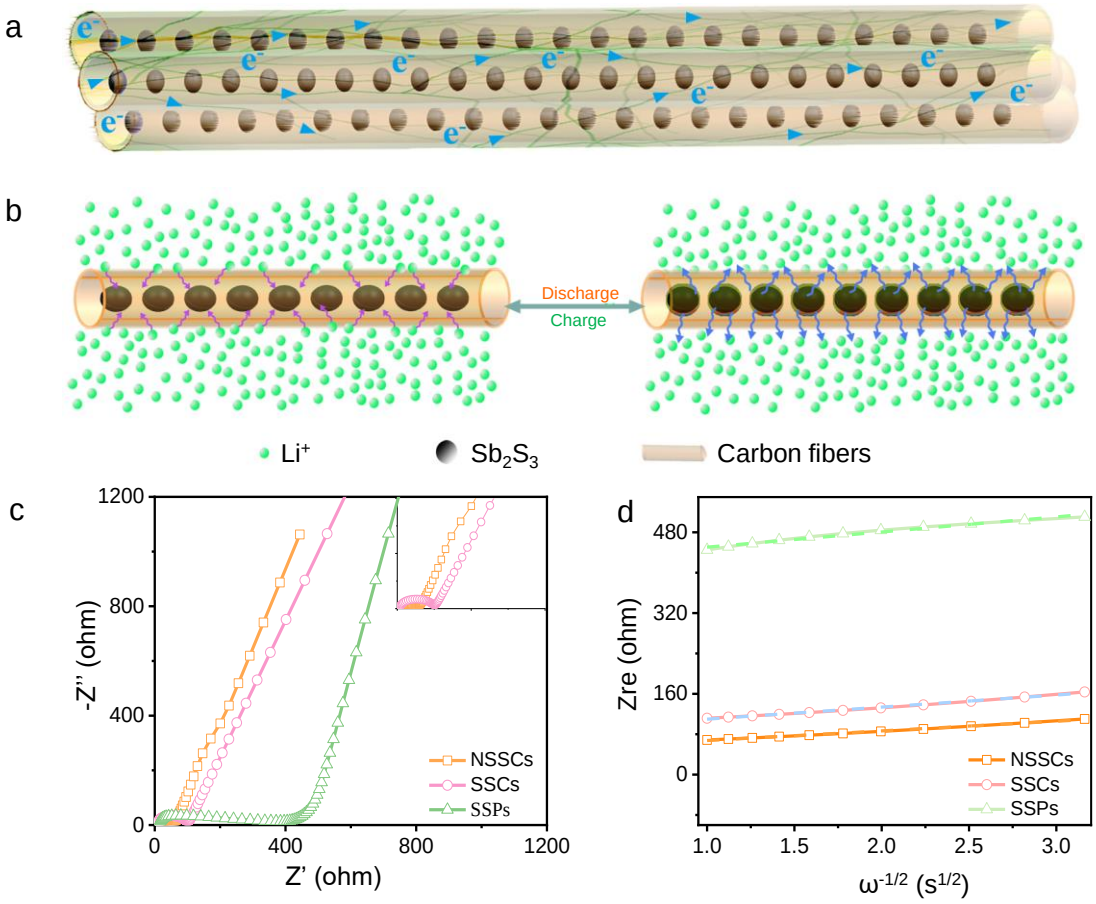

Figure 5. The electronic transfer, Li-ions diffusion and volume expansion mechanism of the N-doped Sb_2S_3 carbon fibers electrode. (a), The schematic of electronic transport in NSSCs electrode. (b), The schematic of Li-ion diffusion in NSSCs electrode. (c), Nyquist plots of the impedance spectra. (d), The real part of complex impedance versus $\omega^{-1/2}$ at open circuit voltage.